 CMC, vol.15, no.3, pp.241-259, 2010

Molecular Dynamics Study of Dynamic Responses of Glassy Silica under Shock Impact

Luming Shen[1]

Abstract: In this study, molecular dynamics (MD) simulations are performed to form glassy silica from melted β-cristobalite using cooling rates of 2, 20 and 200 K/ps. The resulting glassy silica samples are then shocked at particle velocities ranging from 0.3 to 11 km/s in the MD simulations. The effect of the cooling rate on the shock wave velocity is observed for particle velocities below 2 km/s. Moreover, the simulated pressure and density of the shocked glassy silica increase as the cooling rate increases. As compared with the experimental data, the MD simulation can approximately identify the initiation of densification and predict the shock wave velocity within the reasonable accuracy. The simulated pressure and density of the shocked silica match the experimental and EOS analysis data well when the shock pressure is below 500 GPa. However, the proposed MD simulations under-estimate the density when the glass is shocked at pressures above 500 GPa, which indicates that a better interatomic potential model is required for modeling silica under ultrahigh pressures.

Keywords: Glassy silica, shock, molecular dynamics, cooling rate.

1 Introduction

Silica is not only commonly found in nature as sand or quartz but also a principal component of most types of glasses which are used as both window and optical materials. Glass is used as a window material in many applications subject to impact and/or explosion. Hence, it is important to understand the dynamic behavior of glass under low to high velocity impact. On the other hand, due to its significant abundance in the earth mantle, a thorough understanding on the structural and property change of silica under very high pressure is of fundamental importance to the study of the Earth's interior. Hence, the behaviour of silica under very high pressure has been extensively studied, both theoretically and experimentally, over the past

[1] School of Civil Engineering, University of Sydney, NSW 2006 Australia; Email: Luming.Shen@sydney.edu.au

decades [Barmes, Soulard and Mareschal (2006); Lyzenga, Ahrens and Mitchell (1983); Laudernet, Clerouin and Mazevet (2004); Davila, Caturla, Kubota, Sadigh, Diaz de la Rubia, Shackelford, Risbud and Garofalini (2003)]. Meanwhile, fused silica is an important industrial material, particularly for high quality optical elements. For high power lasers commonly used to achieve extreme temperature and pressure conditions, generally transparent optical materials are required to sustain large pressures and temperatures accompanying energy absorption. During such processes, significant damage can be created in the glass optics, in the form of craters which cause the deterioration of the glass optics [Kubota, Caturla, Stölken and Feit (2001); Felter, Hrubesh, Kubota, Davila and Caturla (2003)]. It is therefore necessary to understand the underlying phenomena resulting in the damage of these optical materials under extremely high temperature and pressure.

From the macroscopic point of view, much experimental and numerical research work has been conducted to study the behaviour of silica under shock impact. Wackerle (1963) reported the basic characteristics of compressive wave shapes in fused silica with pressures up to 4 GPa for the first time. Using plate-impact experiments and interferometer instrumentation techniques, Barker and Hollenbach (1970) characterized fused silica as a nonlinear elastic material having the interesting property of propagating stable rarefaction shock waves. Sugiura, Kondo and Sawaoka (1981) studied the permanent densification of fused quartz by using a double stage light-gas gun. They identified the elastic limit of 8.81 GPa and the permanent densification limit of 16 GPa for fused quartz. Experimental data of fused quartz under shock with pressure up to 85 GPa or particle velocity up to 8.5 km/s were also reported in [Marsh (1980)]. Since Brar, Bless and Rosenberg (1991) and Kanel, Rasorenov and Fortov (1992) reported the formation and propagation of failure waves in shocked glass, continued efforts have been made to explore this interesting physical phenomenon [Bourne, Rosenberg and Field (1995); Chen, Feng, Xin and Shen (2003); Shen (2009)].

Compared with macroscopic simulations of materials under impact/shock loading using meshfree particle method [Ma, Zhang, Lian and Zhou (2009); Shen and Chen (2005)], molecular dynamics (MD) are capable of simulating the dynamic behaviors of materials at nanoscale level and providing researchers with molecular details. With ever increasing power of the computers and the significant development of atomistic simulation code, MD has now come of age for shock wave research [Bringa, Rosolankova, Rudd, Remington, Wark, Duchaineau, Kalantar, Hawreliak and Belak (2006); Cao, Bringa and Meyers (2007); Holian (2004)]. To understand the process occurring in the silica due to shock propagation accompanying laser energy absorption, Kubota, Caturla, Stölken and Feit (2001) performed MD simulation of shock wave propagation in silica under piston velocity up to 2.5 km/s

through slabs with up to 240,000 atoms. They observed drastic shock induced modifications in the structure and topology of the SiO_2 network. Barmes, Soulard and Mareschal (2006) used both direct shock propagation with nonequilibrium molecular dynamics (NEMD) at piston velocity up to 5.0 km/s and bulk simulations in the Hugoniot ensemble to characterize the structure and topology of the shocked glass. Their results suggested that above the plastic regime limit, the shock wave would induce profound and irreversible structural changes including the reduction in the average tetrahedral size associated with the material densification. Recently, Alexander, Chhabildas, Reinhart and Templeton (2008) studied the effects of interatomic network structures on the responses of fused silica to low shock pressures. Due to the requirement of using femtosecond time step in the MD, however, the cooling rates applied to form the glassy silica in those MD simulations were several orders of magnitude higher than what used in the reality. Since the structure and topology of the SiO_2 network in the formed glass are dependent on the cooling rate during the glass formation process [Vollmayr, Kob and Binder (1996)], it is essential to investigate how the cooling rate could affect the simulated dynamical responses of the resulting glass under shock impact using MD.

On the other hand, despite significant progress in the understanding of the structure and properties of silica for the solid state near room temperature 300 K and pressures generally below 100 GPa, not much is known, however, on its various behaviour under high pressures (> 100 GPa) and high temperatures (> 5000 K). So far only limited data exist for the Hugoniot of the high pressure fluid phase silica [Hicks, Boehly, Celliers, Eggert, Vianello, Meyerhofer, Collins (2005)]. Using temperature measurements, Lyzenga, Ahrens and Mitchell (1983) observed shock melting of α-quartz under pressure of 110 GPa. Above this pressure silica is expected to transform continuously from a liquid into a dense plasma, a process which has recently been investigated with *ab initio* calculations [Laudernet, Clerouin and Mazevet (2004)]. Using laser-driven shock waves with pressure from 200 to 1,500 GPa, researchers observed the transformation of silica from a liquid near melt into a dense plasma [Hicks, Boehly, Celliers, Eggert, Vianello, Meyerhofer, Collins (2005)].

As can be seen from the open literature, however, no systematic studies have been conducted to study the phase change of glassy silica from elastic regime in solid state to dense plasma under shock pressure ranging from several to a few hundreds GPa. Due to the issues such as large costs, it is not economical in many cases to conduct the real-time tests to investigate the structure and property change of glass under shock, especially for the tests with pressures up to several hundred GPa. In this study, MD simulations are performed to form the silicate glass from β-cristobalite under different cooling rates and the dynamic behavior of the resulting

glassy silica shocked at particle velocities from 0.3 to 11 km/s is then investigated by using MD simulations. The effect of the cooling rate on the dynamical properties of the resulting glassy silica is studied. The simulation results will be verified by the available experimental and theoretical data.

The remaining sections of the paper are arranged as follows. The selection of a suitable interatomic potential model for describing silica is discussed in Section 2, which is followed by the MD simulation of formation of silicate glass from β-cristobalite under different cooling rates in Section 3. The effect of the cooling rate on the structural and property change of the resulting silicate glass shocked at particle velocities up to 11 km/s is studied using MD and the simulation results are compared with available theoretical and experimental data in Section 4. The conclusions are given in the last section.

2 Interatomic potential models

MD simulations require appropriate interatomic potentials that can accurately reproduce the properties and behavior of the materials being investigated [Fitzgerald, Goldbeck-Wood, Kung, Petersen, Subramanian and Wescott (2008); Karki, Bhattarai and Stixrude (2006); Rino, Cardozo and Picinin (2009); Shen and Aduri (2004); Shen and Chen (2004)]. In addition to interactions among silicon and oxygen atoms in silica, the interatomic potential should include Coulombic interactions which require an appropriate method to take the long-range forces into account. Accurate description of silicate glass is not an easy task. Several interatomic potential models have been developed to describe the behavior of silicon dioxide in the glass phase. Herzbach, Binder and Müser (2005) compared three popular interatomic potential models for SiO_2, i.e., the so-called BKS model [van Beest, Kramer and van Santen (1990)], the fluctuating-charge potential model with a Morse stretch term for the short-range interactions (mDCG model) [Demiralp, Cagin and Goddard (1991)], and the polarizable force field (TS model) [Tangney and Scandolo (2002)]. They found that none of the three models can completely outperform the other two in terms of matching the experimental results. The BKS model is thus adopted in this study not only because this model allows for faster simulation than the more complicated three-body model but also it accurately reproduces many thermomechanical properties of different polymorphs [van Beest, Kramer and van Santen (1990)].

The BKS model is a two-body potential based on the Buckingham potential with an added Coulombic term. As discussed in [Barmes, Soulard and Mareschal (2006)], the three body information necessary to create the tetrahedral network in SiO_2 is not lost with the BKS potential, and is implicitly represented by the choice of the potential parameters. In the BKS model the energy of interaction between atoms

depends on three terms: a long range attractive contribution given by a Lennard-Jones form, a short range repulsive part described by an exponential function and a Coulombic contribution. The original BKS potential [van Beest, Kramer and van Santen (1990)] takes the form of

$$V_{ij} = \frac{q_i q_j}{r_{ij}} + A_{ij} e^{-B_{ij} r_{ij}} - \frac{C_{ij}}{r_{ij}^6} \tag{1}$$

where V_{ij} is the potential energy between two atom i and j separated by distance r_{ij}, A_{ij}, B_{ij} and C_{ij} the model parameters, and q_i the charge of atom i. The charges for silicon and oxygen atoms are q_{Si} = 2.4 and q_O = -1.2, respectively. Values for the parameters A_{ij}, B_{ij}, and C_{ij} are given in Tab. 1. All parameters of the BKS potential were found by fitting to both *ab initio* atomistic simulations and experimental data [van Beest, Kramer and van Santen (1990)].

Table 1: Numerical values of the BKS model parameters as proposed in [van Beest, Kramer and van Santen (1990)].

	A_{ij}(eV)	B_{ij}(Å^{-1})	C_{ij}(eV Å^6)
Si-Si	0	1	0
O-O	1388.7730	2.76000	175.0000
Si-O	18003.7572	4.87318	133.5381

Unfortunately, Buckingham-like potentials have the unphysical property of diverging to minus infinity at small interatomic distances [Barmes, Soulard and Mareschal (2006); Vollmayr, Kob and Binder (1996)]. Although this is not a severe drawback at low temperature cases since in order to get to these small distances the particles have to overcome an energy barrier which is, e.g., in the case of the Si-O interaction, on the order of 3,500 K according to our preliminary simulations, it can be disastrous at high temperatures (above 4,000 K) where atoms have the enough kinetic energy to overcome the potential barrier and fuse together. Several methods have been employed to correct for this behaviour. Vollmayr, Kob and Binder (1996) substituted the BKS potential by a harmonic potential when r_{ij} is smaller than the location of the barrier, i.e., for r_{ij} <1.1936 Å and r_{ij} <1.439 Å in the case of the Si-O and O-O interactions, respectively. Barmes, Soulard and Mareschal (2006) replaced the BKS potential with a second order polynomial $V_{ij}(r_{ij})$ for r_{ij} smaller than a certain distance.

In this study, a method similar to that of [Saika-Voivod, Sciortino and Poole (2000)] is used to correct the unphysical behaviour of the BKS model at short range. The

modified BKS potential used in this study takes the form of

$$V_{ij} = \frac{q_i q_j}{r_{ij}} + A_{ij} e^{-B_{ij} r_{ij}} - \frac{C_{ij}}{r_{ij}^6} + D_{oij} \left[e^{-2\alpha_{ij}\left(r_{ij} - r_{0ij}\right)} - 2e^{-\alpha_{ij}\left(r - r_{0ij}\right)} \right] \quad (2)$$

where the first three terms are the same as those in Eq. (1) and the fourth term is a Morse type function added to avoid the fusion of atoms at very short distance. The parameter values are given in Tab. 2. Because of the small D_{oij} and large α_{ij} the added Morse term will not effectively affect the interatomic potential until the interatomic distance is much smaller than r_{oij} (e.g. $r_{SiO} < 1.15$ Å). The Coulombic interactions within distance of 10 Å are computed directly using the first term in Eq. (2), while the long-range Coulombic interactions outside that distance are calculated in reciprocal space using a particle-particle particle-mesh (PPPM) solver [Hockney and Eastwood (1989)], a common technique implemented in many MD simulations. This represents a more accurate modeling of the Coulombic force than that of [Barmes, Soulard and Mareschal (2006)] where the long-range Coulombic interactions are ignored. Since the structure of SiO_2 is essentially controlled by the interactions within the shell of first neighbours [Barmes, Soulard and Mareschal (2006)], a cut off of 8 Å is applied to the second and third terms in Eq. (2).

Table 2: Numerical values of the modified BKS model parameters in Eq. (2).

	D_{oij}(eV)	r_{oij} (Å)	α_{ij} (Å^{-1})
Si-Si	0	2.0	0
O-O	0.0001	1.7792	20.0
Si-O	0.0002	1.3136	20.0

3 Formation of glassy silica

The common approach to forming a glassy silica sample in MD simulation is to melt a crystal silica at very high temperature (say 7000 K) and then cool the liquid phase SiO_2 past the liquid to glass transition point [Barmes, Soulard and Mareschal (2006); Kubota, Caturla, Stölken and Feit (2001);]. As demonstrated in [Vollmayr, Kob and Binder (1996)], the cooling rate is an important parameter since the resulting glass structure is heavily dependent on the formation history. Due to the very small time step required in the MD simulations, even the slowest cooling rates achievable with today's computers are several orders of magnitude greater than the fastest cooling rates used in experiments. As a result much higher glass transition temperatures are expected from the MD simulations [Barmes, Soulard and

Mareschal (2006); Vollmayr, Kob and Binder (1996)], which would in turn affect the dynamic response of the resulting glass sample under shock pressure.

In this study, a series of MD simulations using code LAMMPS [Plimpton (1995)] are performed to create a silica system in the glass phase under different cooling rates. The glass sample preparation starts from β-cristobalite with initial mass density of 2.2 g/cm^3. The dimensions of the initial simulation box are 33.9 Å $\times$ 33.9 Å $\times$ 509.1 Å. The total number of atoms in the simulation is 38,880. Periodic boundary conditions (PBCs) are applied in all three directions. In order to remove all memory from the initial crystal structure, the system is melted under pressure P = 0 GPa and temperature T = 7,000 K using *NPT* ensemble for 210 ps. To avoid any atoms flying away from the system, a very small time step 0.1 fs is used in the first 10 ps. A larger time step 0.5 fs is applied after that. The Nose/Hoover temperature thermostat and pressure barostat are used to keep the constant temperature and pressure, respectively. After the 210 ps melting period at T = 7,000 K, the liquid glass is then cooled down to T= 300 K at a cooling rate of 200K/ps, 20 K/ps or 2 K/ps. The system is relaxed at 300 K for another 50 ps. Note these cooling rates are still orders higher than what used in the experiments.

The dimensions of the resulting glassy silica systems under cooling rates of 200 K/ps, 20 K/ps and 2 K/ps are 32.2Å $\times$ 32.2Å $\times$ 483.3Å, 32.4Å $\times$ 32.4Å $\times$ 486.5Å and 32.5Å $\times$ 32.5Å $\times$ 488Å, respectively. The density of the formed glass sample decreases from 2.569 g/cm^3 to 2.497 g/cm^3 when the cooling rate deceases from 200 K/ps to 2 K/ps. Although the simulated densities are about 13.5% to 16.8% larger than the experimental value of 2.20 g/cm^3, it seems the density of the simulated silicate glass can be reduced down to the experimental value when a much slower cooling rate is adopted. The effect of the cooling rate on the long structure of the resulting glass is studied through the radial distribution function $g(r)$. Fig. 1 shows the radial distribution functions for Si-Si, Si-O and O-O in glassy silica cooled down from 7,000 K to 300 K at different rates. It can be seen from the figure that the phase of the sample changes from the liquid state under the melting temperature of 7,000 K to the amorphous structure at 300 K. The first peaks for the Si-Si, Si-O and O-O pairs at T = 300 K are at r_{SiSi} = 3.10 Å, r_{SiO} = 1.65 Å and r_{OO} = 2.60 Å, respectively. These match with the experimental values r_{SiO} = 1.61 Å and r_{OO} = 2.63 Å [Johnson, Wright and Sinclair (1983); Mozzi and Warren (1969)] and simulated value r_{SiSi} = 3.05 Å using MD with a three-body potential [Vashishta, Kalia, Rino and Ebbsjö (1990)]. Although the position of the first peak for the Si-Si, Si-O or O-O pair does not depend on the cooling rate, the g(r) values of both the Si-Si and O-O pairs at their first peak position do increase as the cooling rate decreases, indicating a more crystal-like structure might be formed under a lower cooling rate.

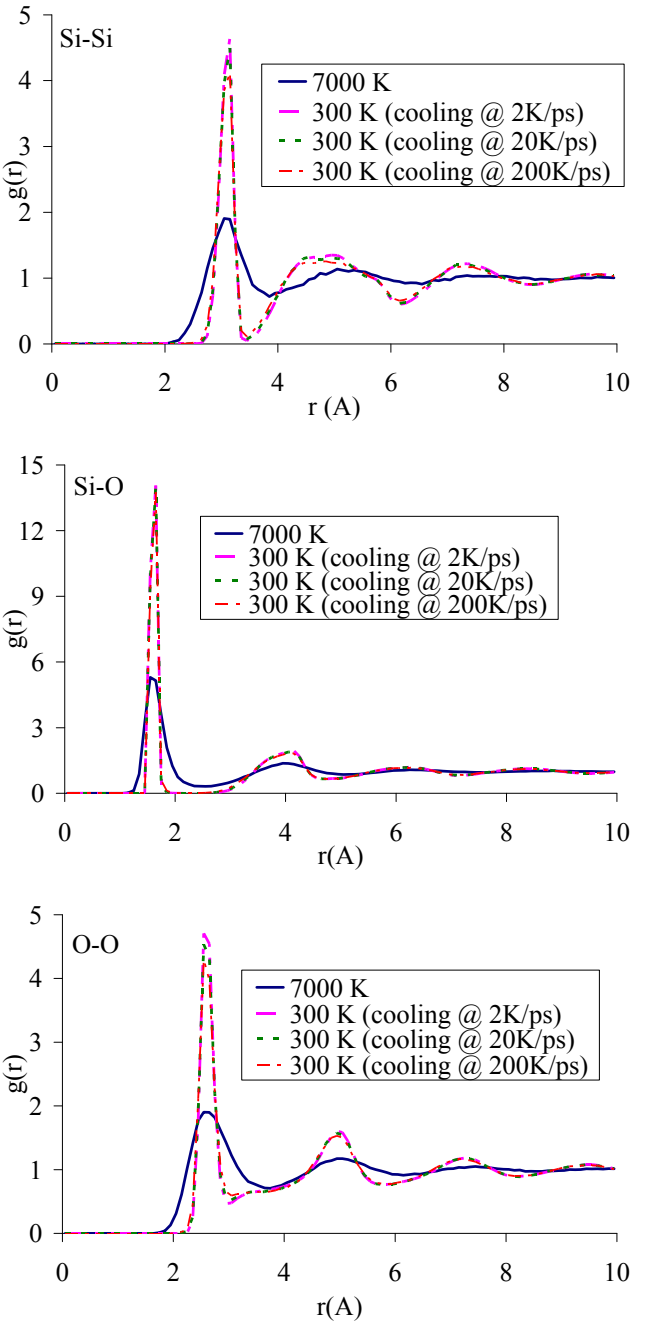

Figure 1: The effect of cooling rate on the radial distribution functions for Si-Si, Si-O and O-O pairs in the glass phase.

4 Glassy silica under shock

The dynamic responses of the resulting silicate glass samples under shock are then investigated through a NEMD simulation. In the beginning of the simulation, free surfaces are created on the both ends in the longitudinal direction of the resulting glassy SiO_2, while PBCs are enforced along the other two directions at 300 K. The inaccuracy in calculating the long-range Coulombic interactions caused by the free surfaces can be neglected since the Coulombic force at this distance ($\sim$500 Å) will be almost zero. In the proposed NEMD simulations, LAMMPS is adopted with a time step of 0.1-0.5 fs depending on the particle velocity. All the MD simulations are performed using NVE ensembles.

In order to generate the shock wave, a constant velocity u is applied to the set of atoms within a distance of 7-90 Å from the left end throughout the simulation. This set of atoms will act as a piston travelling at a fixed velocity u. Movement of these atoms will induce the propagation of a mechanical shock wave through the sample at velocity Dwhich is a function of both u and equation of state of the system. The shock wave divides the system into two parts: the non-shocked region, which is located downstream of the shock wave, and the shocked region, located upstream of the shock wave. A reflecting wall is imposed at the right end where all atoms will bounce back at the velocities same as their incoming velocities. The initial set-up of the simulation is demonstrated in Fig. 2(a). Figs 2(b)-(d) demonstrate the propagation of a shock wave from the left to the right under particle velocity of 4.0 km/s in the glass sample formed under cooling rate of 20 K/ps. The shock front could be clearly identified at the transition of image darkness.

To investigate the dynamic responses of glass under shock, the silicate glass sam-

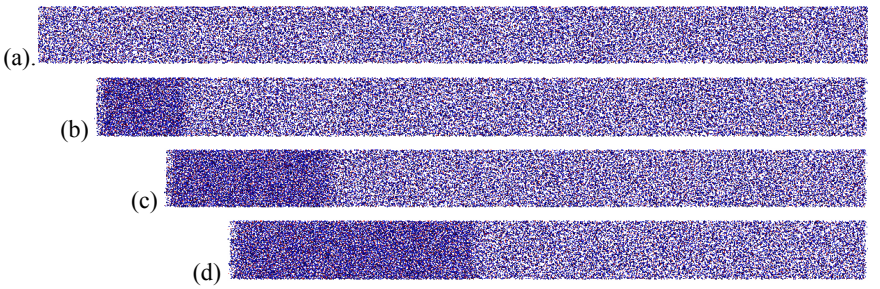

Figure 2: Configuration of the silicate glass formed at cooling rate of 20 K/ps shocked under piston velocity u = 4.0 km/s at time (a) t=0, (b) t =1 ps, (c) t =2 ps and (d) t =3 ps.

ples created under different cooling rates are shocked at different particle velocities in the NEMD. The shock wave velocities are derived from the velocity profiles of the atoms as a function of depth at different times. Fig. 3 shows a set of velocity profiles in the glass sample formed under cooling rate of 20 K/ps for the cases of particle velocities of (a) 1.0 km/s, (b) 2.0 km/s, (c) 3.0 km/s and (d) 4.0 km/s at different times. The pressure and mass density profiles of the same silicate glass shocked at particle velocity of 4.0 km/s at different times are presented in Fig. 4. As can be seen from Figs. 3 and 4, the shapes of the profiles for the intermediate times do not change in time, indicating a stable shock wave front. At long times when the wave reaches the fixed right end and bounces back, the cancellation of the incoming particle velocity by the reflection wave can be clearly seen in Fig. 3(d), which is consistent with the sudden increase in pressure and mass density of glass in Fig. 4(a) and Fig. 4(b), respectively.

The differences between velocity profiles at different times corresponding to a value of half of the maximum particle velocity is computed in order to obtain the shock wave velocity. Fig. 5 presents the shock wave velocity$D$ as a function of the particle velocity u for glass samples formed under cooling rates of 200 K/ps, 20 K/ps and 2 K/ps. As can be seen from the $D-u$ curve for the glass sample formed under cooling rates of 2 K/ps and 20 K/ps in Fig. 5, there are two different regimes in the shock wave velocities. At particle velocities less than 1.0 km/s the elastic region is observed, where the shock velocity slightly decreases with the increasing particle velocity, and then there is an obvious decrease in shock wave velocity at about particle velocity of 1.0-1.4 km/s. The shock wave velocity starts to increase linearly with increasing particle velocity at 1.4 km/s, which defines the initiation of densification regime. This is consistent with the MD simulation results in references [Kubota, Caturla, Stölken and Feit (2001); Davila, Caturla, Kubota, Sadigh, Diaz de la Rubia, Shackelford, Risbud and Garofalini (2003)]. For comparison, experimental results in [Sugiura, Kondo and Sawaoka (1981); Marsh (1980)] are also presented in Fig. 5. It can be seen from the figure that the MD simulations for the glass formed under cooling rates of 2 K/ps and 20 K/ps are able to qualitatively reproduce the transition from the elastic limit into densification regime at particle velocity of around 1.0-1.4 km/s [Sugiura, Kondo and Sawaoka (1981)]. However, such transition can not be clearly observed from the $D-u$ curve of the glass sample formed under cooling rates of 200 K/ps. Instead the elastic wave velocity is much lower for u < 1.0 m/s and the shock wave velocity starts to increase at u = 1.2km/s.

For 1.4m/s < u < 5m/s the experimentally measured shock velocities [Sugiura, Kondo and Sawaoka (1981); Marsh (1980)] are slightly lower than those simulated, which do not vary much with the cooling rate and increase linearly with the

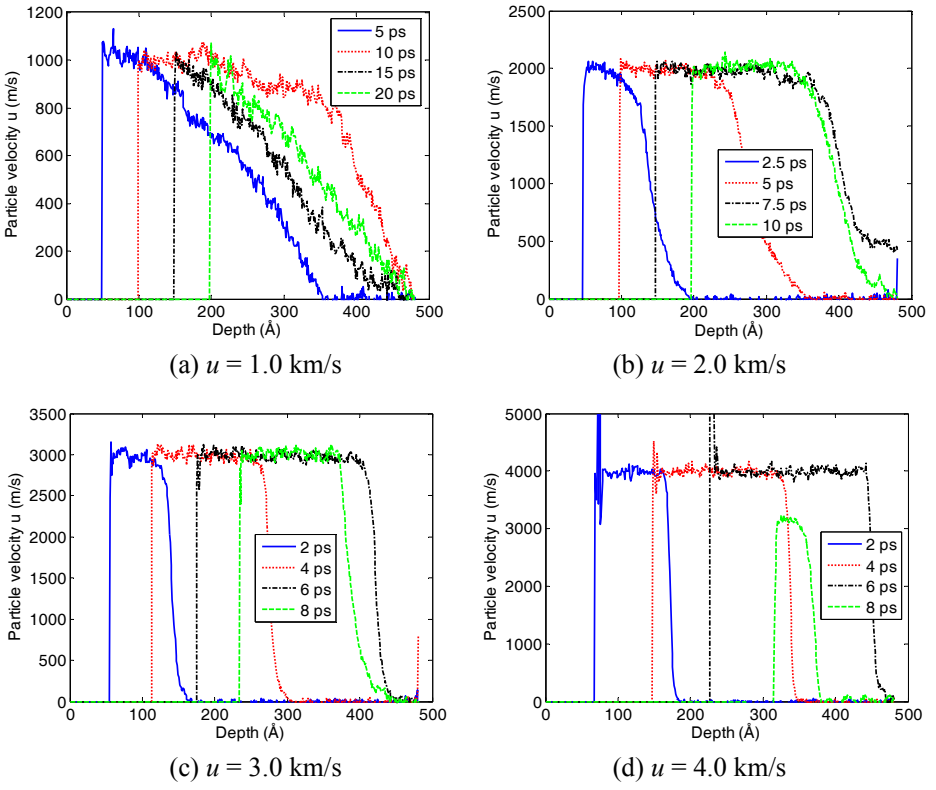

(a) u = 1.0 km/s (b) u = 2.0 km/s

(c) u = 3.0 km/s (d) u = 4.0 km/s

Figure 3: Velocity profiles in the glassy silica formed at cooling rate of 20 K/ps under particle velocities of (a) 1.0 km/s, (b) 2.0 km/s, (c) 3.0 km/s and (d) 4.0 km/s at different times.

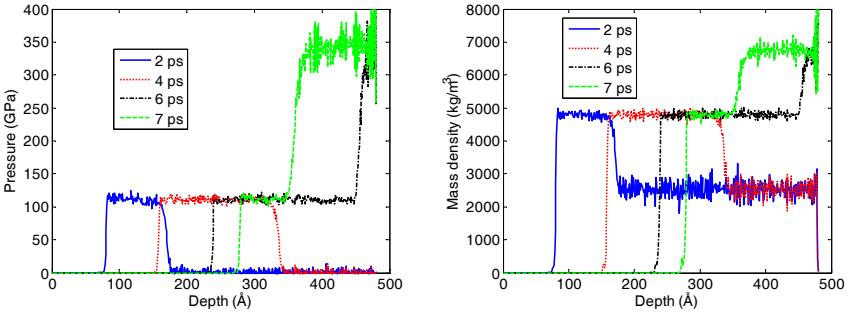

(a) pressure profiles (b) mass density profiles

Figure 4: (a) Pressure and (b) mass density profiles of silicate glass formed at cooling rate of 20 K/ps under particle velocity of 4.0 km/s at different times.

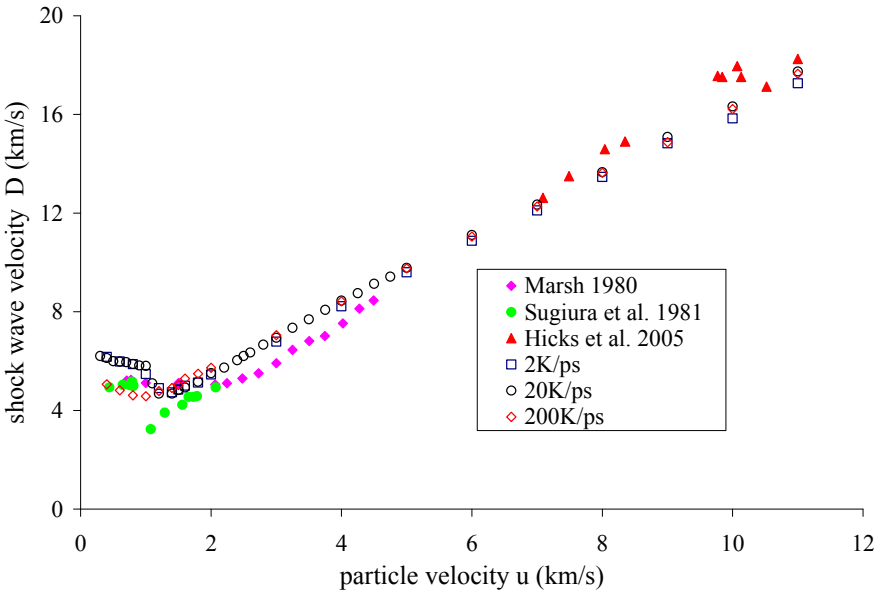

Figure 5: Velocities of shock wave as a function of particle velocities from MD simulations and experiments.

particle velocity, as shown in Fig. 5. It shows that for $u > 5$m/s the simulated shock velocities match the experimentally measured data in [Hicks, Boehly, Celliers, Eggert, Vianello, Meyerhofer, Collins (2005)] well. It suggests from Fig. 5 that the cooling rate do have certain effect on the $D-u$ relationship, in particular, for $u <$ 1.4 km/s where the transition from the elastic limit into densification regime exists. Above that pressure point, no significant cooling rate effect on the shock wave velocity is observed except that the simulated shock wave velocity increases slightly with the cooling rate. In general, the simulated shock wave velocity can effectively predict the experimental data.

Figure 6 shows the relationship between the simulated density ρ and particle velocity u for the glass samples formed under different cooling rates. As can be seen the figure, the mass density ρ is smaller for the glass sample created under a lower cooling rate regardless of the particle velocity. Fig. 6 also compares the simulated densities at different particle velocities with available experimental data [Sugiura, Kondo and Sawaoka (1981); Marsh (1980); Hicks, Boehly, Celliers, Eggert, Vianello, Meyerhofer, Collins (2005)]. It can be seen from Fig. 6 that the agreement between the simulated mass density and the measured values under par-

ticle velocity of 10 km/s is acceptable. However, the difference becomes obvious when the particle velocity increases further. As can be seen from Fig. 6, when the particle velocity increases further beyond 11 km/s, no significant increase of the simulated glass density is observed, while the experimental data show an increase of mass density of the shocked silica.

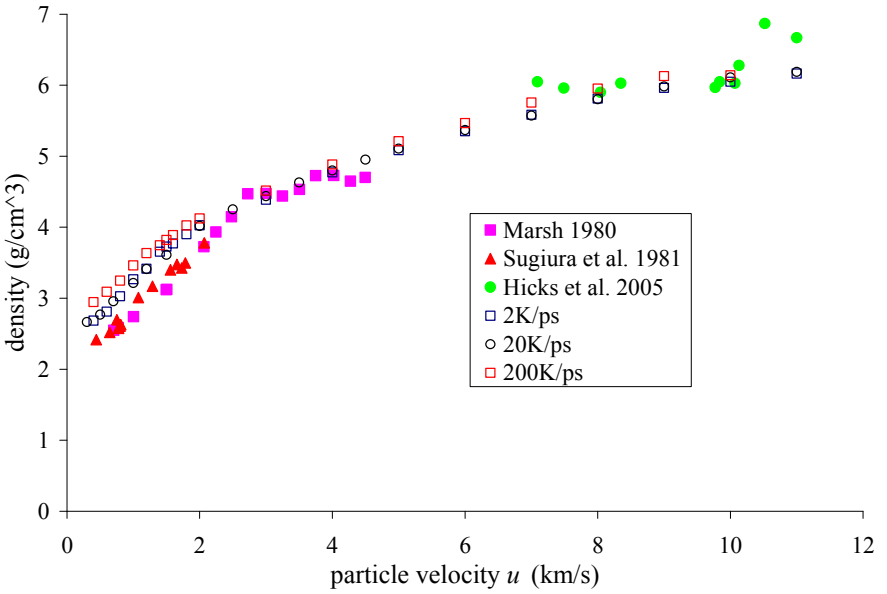

Figure 6: Densities of silicate glass as a function of particle velocities from MD simulations and experiments.

The simulated incompressibility of silica under ultra-high shock pressures could be due to two reasons. First, in the MD simulations ultrahigh pressures are achieved in about one picosecond, which is about 2-3 orders shorter than the time duration sustained by the laser-driven shocks in experiments [Hicks, Boehly, Celliers, Eggert, Vianello, Meyerhofer and Collins (2005)]. Hence, the simulated states under ultrahigh pressures might not be at equilibrium. Kubota, Caturla, Stölken and Feit (2001) have demonstrated that the number of five-fold and three-fold coordinated silicon atoms decreased dramatically after the shocked glass has been relaxed for about 33 picoseconds, which is still a very short relaxation time as compared to the nanosecond time duration in the laser-driven shocks. Hence, the simulated glass shocked under ultrahigh pressure states might not be at equilibrium. A larger and longer glass sample, which allows for a longer simulation time, might be needed

in order to enable the shocked glass to reach its equilibrium condition. Second, as demonstrated by Hicks, Boehly, Celliers, Eggert, Vianello, Meyerhofer and Collins (2005), with the increasing shock pressure the silica will transform from solid state ($p < 100$ GPa), dissociating liquid state ($100 < p < 400$ GPa) to dense plasma ($p > 400$ GPa). The original BKS model was not specially developed for simulating the thermodynamic responses of plasma phase silica. Moreover, the Morse type function in Eq. (2) added to avoid the fusion of atoms at very short distance might also contribute to the unphysical incompressibility of silica at extremely high pressure. Hence, the potential model requires further improvement in order to better model silicate under dense plasma state.

Figure 7 demonstrates the relationship between the shock pressure p and the density of shock glass. As can be seen from the figure, the simulated p-ρ curve matches the experimental measurements relatively well up to shock pressure of $\sim$500 GPa. Above that pressure level, the simulated results start to deviate from the experimental data [Hicks, Boehly, Celliers, Eggert, Vianello, Meyerhofer and Collins (2005)]. The increasing deviation of the simulated results from the experimental data under ultrahigh shock pressures could be caused by the poor potential model for silica under ultrahigh pressure and the non-equilibrium states achieved in the MD simulations.

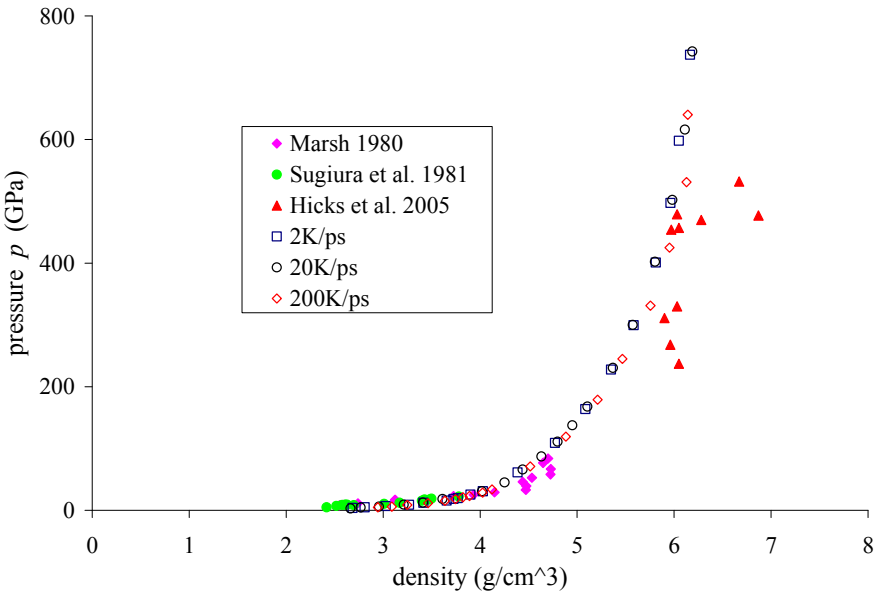

Figure 7: Shock pressure vs. density of glassy silica.

The thermodynamical quantities obtained from the proposed MD simulations are also compared with available data from the SESAME Equation-of-State (EOS) Library. For the purpose of simplicity, some SESAME EOS data published in Table I of [Laudernet, Clerouin and Mazevet (2004)] are adopted. The MD simulation results obtained from the glass sample formed under cooling rate of 20 K/ps are presented as well. The comparison is shown in Tab. 3, where p_{eos}, ρ_{eos} and T_{eos}, and ρ_{MD}, p_{MD} and T_{MD} represent pressure, density and temperature obtained from the SESAME EOS analysis and current MD simulations, respectively. As can be seen from Tab. 3, the simulated density matches that of EOS analysis for pressure below 500 GPa well. Due to the limitation of the BKS potential model and the non-equilibrium state achieved in the MD, the current simulation underestimates the density of silicate for pressure over 500 GPa and the proposed MD simulation slightly underestimates the temperature of silica under shock.

Table 3: Comparison between the SESAME and MD thermodynamical quantitiesp_{eos}, ρ_{eos} and T_{eos}, and ρ_{MD}, p_{MD} and T_{MD}, respectively.

p_{eos} (GPa)	ρ_{eos} (g/cm^3)	T_{eos} (K)	p_{MD} (GPa)	ρ_{MD} (g/cm^3)	T_{MD} (K)
100	4.71	7700	99.1	4.716	5855
200	5.04	16000	231	5.369	12852
500	5.83	38700	502	5.982	30829

5 Conclusions

In this study, a modified BKS model with the consideration of long-range Coulombic interactions is used to model the interatomic interactions among silicon and oxygen atoms in the silica. MD simulations are performed to form glassy silica by melting β-cristobalite at temperature 7,000 K and cooling the liquid glass down to room temperature 300 K at a cooling rate of 200 K/ps, 20 K/ps or 2 K/ps. The density of the resulting silicate glass sample is 13.5-16.8% higher than the experimental value and it decreases with the cooling rate. It is believed that the higher density of the simulated glass could be caused by the extremely high cooling rate used in the MD simulations, which cannot be avoided at this stage because of the limited computing capability. However, the radial distribution functions of the simulated glass match the available experimental data and other MD simulation results well.

The resulting glassy silica samples are then shocked at particle velocities ranging from 0.3 km/s to 11 km/s in the MD simulations. The effect of the cooling rate on the shock wave velocity is observed for particle velocities below 2 km/s. Moreover,

the simulated pressure and density of the shocked glass increase as the cooling rate increases. As compared with the experimental data, the MD simulation can approximately identify the initiation of densification and predict the shock wave velocity within the reasonable accuracy. The simulated pressure and density of the shocked glass match the experimental and EOS analysis data well when the pressure is below 500 GPa. However, the proposed MD simulations under-estimate the density when the glass is shocked at pressures above 500 GPa.

The increasing disagreements between the simulated results and the experimental data for silica under ultra-high shock pressures could be due to two reasons. First, since the ultrahigh pressures are achieved in about one picosecond in the MD simulations, the simulated states might not be at equilibrium. Second, the original BKS model was not specially developed for simulating the thermodynamic responses of silica under ultrahigh pressures. Moreover, the Morse type function added to avoid the fusion of atoms at very short distance might also contribute to the unphysical incompressibility of plasma phase silica. The improvement of the potential model is required in order to better model silicate under dissociating liquid and dense plasma states. Further study on this particular issue is currently underway.

Acknowledgement: The work was supported in part by the Australian Research Council under Grant No DP0772478. All the MD simulations were carried out on the supercomputers in the Victorian Partnership for Advanced Computing (VPAC) in Australia, the Australian Centre for Advanced Computing and Communications (ac3), and the NCI National Facility in Australia. Fig. 2 was produced by utilizing software VMD [Humphrey, Dalke and Schulten (1996)].

References

Alexander, C.S.; Chhabildas, L.C.; Reinhart, W.D.; Templeton, D.W. (2008): Changes to the shock response of fused quartz due to glass modification. *Int. J. Impact Eng.*, vol. 35, pp. 1376-1385.

Barker, L.M.; Hollenbach, R.E. (1970): Shock-wave studies of PMMA, fused silica and sapphire. *J. Appl. Phys.,* vol. 41, pp. 4208-4226.

Barmes, F.; Soulard, L.; Mareschal, M. (2006): Molecular dynamics of shock-wave induced structural changes in silica glasses. *Phys. Rev.* B, vol. 73, pp. 224108.

van Beest, B.W.H.; Kramer, G.J.; van Santen, R.A. (1990): Force fields for silicas and aluminophosphates based on ab initio calculations. *Phys. Rev. Lett.,* vol. 64, pp. 1955-1958.

Bourne, N.K.; Rosenberg, Z.; Field, J.E. (1995): High-Speed Photography of

Compressive Failure Waves in Glasses. *J. Appl. Phys.*, vol. 78, pp. 3736-3739.

Brar, N.S.; Bless, S.J.; Rosenberg, Z. (1991): Impact-induced failure waves in glass bars and plates. *Appl. Phys. Lett.,* vol. 59, pp. 3396-3398.

Bringa, E.M.; Rosolankova, K.; Rudd, R.E.; Remington, B.A.; Wark, J.S.; Duchaineau, M.; Kalantar, D.H.; Hawreliak, J.; Belak, J. (2006): Shock deformation of face-centred-cubic metals on subnanosecond timescales. *Nature Mater.,* vol. 5 pp., 805-809.

Cao, B.; Bringa, E.M.; Meyers, M.A. (2007): Shock compression of monocrystalline copper: atomistic simulations. *Metall. Mater. Trans.* A, vol. 38, pp. 2681-2688.

Chen, Z.; Feng, R.; Xin, X.; Shen, L. (2003): A computational model for impact failure with shear-induced dilatancy. *Int. J. Num. Meth. Eng.,* vol. 56, pp. 1979–1997.

Davila, L.P.; Caturla, M.J.; Kubota, A.; Sadigh, B.; Diaz de la Rubia, T.; Shackelford, J.F.; Risbud, S.H.; Garofalini, S.H. (2003): Transformations in the medium-range order of fused silica under high pressure, *Phys. Rev. Lett.,* vol. 91, pp. 205501.

Demiralp, E.; Cagin, T.; Goddard, W.A. (1991): Morse stretch potential charge equilibrium force field for ceramics: application to the quartz-stishovite phase transition and to silica glass. *Phys. Rev. Lett.,* vol. 82, pp. 1708–1711.

Felter, T.E.; Hrubesh, L.; Kubota, A.; Davila, L.P.; Caturla, M.J. (2003): Laser damage probability studies of fused silica modified by MeV ion implantation. *Nucl. Instr. Meth.* B, vol. 207, pp. 72-79.

Fitzgerald, G; Goldbeck-Wood, G; Kung, P.; Petersen, M.; Subramanian, L.; Wescott, J. (2008): Materials modeling from quantum mechanics to the mesoscale. *CMES-Computer Modeling in Engineering & Sciences*, vol. 24, pp. 169-183.

Herzbach, D.; Binder, K.; Müser, M.H. (2005): Comparison of model potentials for molecular-dynamics simulations of silica. *J. Chem. Phys.,* vol. 123, no. 124711.

Hicks, D.G.; Boehly, T.R.; Celliers, P.M.; Eggert, J.H.; Vianello, E.; Meyerhofer, D.D.; Collins, G.W. (2005): Shock compression of quartz in the high-pressure fluid regime. *Phys. Plasmas*, vol. 12, no. 082702.

Hockney, R.W.; Eastwood, J.W. (1989): *Computer Simulation Using Particles*, Adam Hilger, NY.

Holian, B.L. (2004): Molecular dynamics comes of age for shockwave research. *Shock Waves*, vol. 13, pp. 489-495.

Humphrey, W.; Dalke, A.; Schulten, K. (1996): VMD-visual molecular dynam-

ics. *J. Mol. Graph.,* vol. 14, pp. 33-38.

Johnson, P.A.V.; Wright, A.C.; Sinclair, R.N. (1983): Neutron scattering from vitreous silica II. Twin-axis diffraction experiments. *J. Non-Crystalline Solids,* vol. 58, pp. 109-130.

Kanel, G.I.; Rasorenov, S.V.; Fortov, V.E. (1992): The failure waves and spallations in homogeneous brittle materials. *Shock Compression of Condensed Matter–1991* (Edited by Schmidt SC, Dick RD, Forbes JW, Tasker DG). Elsevier, New York, 451-454.

Karki, B.B.; Bhattarai, D.; Stixrude, L. (2006): A first-principles computational framework for liquid mineral systems. *CMC: Computers, Materials & Continua*, vol. 3(3), pp. 107-117.

Kubota, A.; Caturla, M.J.; Stölken, J.S.; Feit, M.D. (2001): Densification of fused silica due to shock waves and its implications for 351 nm laser induced damage. *Opt. Express*, vol. 8, pp. 611-616.

Laudernet, Y.; Clerouin, J.; Mazevet, S. (2004): ab initio simulations of the electrical and optical properties of shock-compressed SiO_2. *Phys. Rev.* B, vol.70, pp. 165108.

Lyzenga, G.; Ahrens, T; Mitchell, A. (1983): Shock temperatures of SiO_2 and their geophysical implications. *J. Geophys. Res.,* vol. 88, pp. 2431-2444.

Ma, S.; Zhang, X.; Lian, Y.; Zhou, X. (2009): Simulation of high explosive explosion using adaptive material point method, *CMES: Computer Modeling in Engineering & Sciences,* vol. 39(2), pp. 101-124.

Marsh, S.P. (1980): *LASL Shock Hugoniot Data*. University of California Press.

Mozzi, R.L.; Warren, B.E. (1969): The structure of vitreous silica. *J. Appl. Crystallography*, vol. 2, pp. 164-172.

Plimpton, S.J. (1995): Fast parallel algorithms for short-range molecular dynamics. *J. Comput. Phys.*, vol. 117, pp. 1-19.

Rino, J.P.; Cardozo, G.D.; Picinin, A. (2009): Atomistic Modeling of the Structural and Thermal Conductivity of the InSb. *CMC: Computers, Materials & Continua,* vol. 12(2), pp. 145-156.

Saika-Voivod, I.; Sciortino, F.; Poole, P.H. (2000): Computer simulations of liquid silica: Equation of state and liquid-liquid phase transition. *Phys. Rev.* E, vol. 63, no. 011202.

Shen, L. (2009): A rate-dependent damage/decohesion model for simulating glass fragmentation under impact using the material point method. *CMES: Computer Modeling in Engineering & Sciences*, vol. 49, pp. 23-45.

Shen, S.P.; Aduri, S.N. (2004): Computational nano-mechanics and multi-scale simulation. *CMC: Computers, Materials & Continua*, vol. 1(1), pp. 59-90.

Shen, L.; Chen, Z. (2004): An investigation of the effect of interfacial atomic potential on the stress transition in thin films. *Modelling Simulation in Materials Science and Engineering*, vol. 12 (4), pp. S347-S369.

Shen, L.; Chen, Z. (2005): A silent boundary scheme with the material point method for dynamic analyses. *CMES: Computer Modeling in Engineering & Sciences*, vol.7(3), pp. 305-320.

Sugiura, H.; Kondo, K.; Sawaoka, A. (1981): Dynamic response of fused quartz in the permanent densification region. *J. Appl. Phys.*, vol. 52, pp. 3375-3382.

Tangney, P.; Scandolo, S. (2002): An ab initio parameterized interatomic force field for silica. *J. Chem. Phys*., vol. 117, pp. 8898-8904.

Vashishta, P.; Kalia, R.K.; Rino, J.P.; Ebbsjö, I. (1990): Interaction potential for SiO_2: A molecular-dynamics study of structural correlations. *Phys. Rev.* B, vol. 41 pp. 12197–12209.

Vollmayr, K.; Kob, W.; Binder, K. (1996): Cooling-rate effects in amorphous silica: A computer-simulation study. *Phys. Rev.* B, vol. 54, pp. 15808-15827.

Wackerle, J. (1963): Shock-wave compression of quartz. *J. Appl. Phys.,* vol. 33, pp. 922-937.